Scientia Iranica, Vol. 11, Nos. 1&2, pp 60–68

SCIENTIA IRANICA

Three-Dimensional Eigenmode Flutter Analysis of a Rectangular Cantilever Plate in Low Subsonic Flow

F. Bakhtiari Nejad* **and S. Shokrollahi**[1]

In this paper, a 3-D, unsteady vortex lattice model to compute aerodynamic coefficients, using time domain eigenmode analysis, is presented. A computationally efficient technique for constructing a reduced order model of unsteady flow about a low aspect ratio wing, modeled as a cantilever plate of constant thickness, is presented. Analysis demonstrates that limit cycle oscillations of the order of the plate thickness are possible. The eigenmodes of the system, which may be considered as aerodynamic states, are computed and, subsequently, used to construct a computationally efficient, reduced order model of an unsteady flowfield. Only a handful of the most dominant eigenmodes are retained in the reduced order model. The effect of the remaining eigenmodes is included approximately, using a static correction technique. An advantage of the present method is that, once the eigenmode information has been computed, the reduced order model can be constructed for any number of arbitrary modes of wing motion very inexpensively. The method is particularly well suited for use in the active control of aeroelastic phenomena, as well as in standard aeroelastic analysis for flutter or gust response. Finally, a numerical example is presented that demonstrates the accuracy and computational efficiency of the present method.

INTRODUCTION

In recent years, significant progress has been made in the development of unsteady aerodynamic analysis to predict the flutter and forced response of airfoils, wings and even complete aircraft configuration.

Most unsteady aerodynamic modeling can be obtained by two main groups; time domain and frequency domain analyses. In time domain analysis, one discretizes the governing equations on a computational mesh and then marches the solution from one time step to the next. At each time step, one imposes boundary conditions arising from either the prescribed motion of the airfoil or wing. For example, Davis and Bendiksen [1] have time marched two-dimensional Euler equations to find the unsteady flow about vibrating airfoils. Batina [2] has computed the time dependent Euler flow about a complete harmonically deforming aircraft. Chaderjian and Guruswamy [3] have applied the time marching technique to solve transonic Navier-Stokes equations about an oscillating wing. Deman Tang et al. [4] have applied a 2D vortex Lattice model to compute aerodynamic coefficients in a 3-dimensional flowfield.

In this paper, a 3-D unsteady vortex lattice model is applied to compute aerodynamic coefficients, using time domain analysis.

Time domain analyses, although able to model extremely complex flow features and nonlinear effects, are computationally expensive, due to the requirement of the solutions to be both accurate and stable. In frequency domain analyses, one assumes that the unsteadiness is small compared to the mean flow. Thus, the unsteady flow is governed by linear small disturbance equations. The unsteady motion is assumed to be harmonic in time ($e^{i\omega t}$), so that the time derivative operator, $\frac{\partial}{\partial t}$, is replaced by $i\omega$. Hence, time does not appear explicitly in the governing equations. One of the main difficulties with both time domain and frequency domain techniques is that a separate analysis must be performed for each frequency and mode shape of interest. Unfortunately, in aeroelastic calculations, the

*. *Corresponding Author, Solid Mechanics Center, Department of Mechanical Engineering, Amir Kabir University of Technology, Tehran, I.R. Iran.*

1. *Department of Mechanical Engineering, Amir Kabir University of Technology, Tehran, I.R. Iran.*

frequencies and mode shapes are often not known a priori. A number of investigators have circumvented this difficulty by simultaneously marching the fluid and structural dynamic equations of motion. This approach, although relatively straightforward, is still, computationally, very expensive. Furthermore, separate analysis must be performed for each reduced velocity or mass ratio of interest. Finally, for applications to active control problems, such simulations do not provide the control engineers with the Laplace plane information needed to formulate control laws. One approach to overcoming these difficulties is to develop reduced order models of time domain or frequency domain aerodynamic analyses. The goal is to describe the unsteady aerodynamic loads over a range of reduced frequencies, using models with a small number of aerodynamic states. One way to do this is to simply evaluate the unsteady load, due to a particular mode shape of vibration, at a number of reduced frequencies and, then, curve fit the results to a convenient time domain representation. The approximate time domain representation is usually taken to be a sum of exponentials, since the corresponding Laplace transform is a rational polynomial. The parameters in the approximation, such as the time constant of the exponentials or the constant multiplying of each exponential, are found by minimizing the error between the approximation and the exact solutions at a finite number of frequencies. Note that this method requires the approximation for the unsteady aerodynamic loads to be computed for each mode shape of the vibrating wing.

AERODYNAMIC EQUATIONS : VORTEX LATTICE MODEL

The flow about the cantilever plate is assumed to be incompressible, inviscid and irrotational. Hence, the unsteady flowfield may be modeled using potential flow techniques. Here, an unsteady vortex lattice method is used to model this flow. A typical planar vortex lattice mesh for the three-dimensional flow is shown in Figure 1. The plate and wake are divided into a number of elements. All of the elements on the wing and wake are of equal size, Δx, in the streamwise direction. Point vortices are placed on the plate and in the wake at the quarter chord of the elements. At the three-quarter chord of each plate element, a collocation point is placed for the downwash, i.e., the velocity induced by the discrete vortices is required to equal the downwash arising from the unsteady motion of the plate. Thus, one obtains the relationship:

$$w_i^{t+1} = \sum_j^{kmm} K_{ij}\Gamma_j^{t+1} \quad i = 1, ..., km, \tag{1}$$

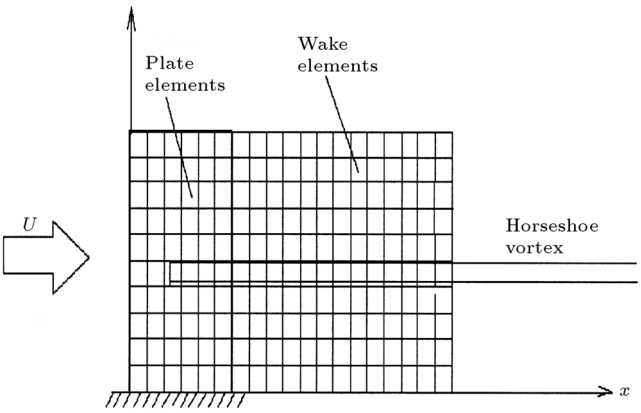

Figure 1. Three-dimensional aeroelastic model of a cantilever plate.

where w_i^{t+1} is the downwash at the ith collocation point at time step $t+1, \Gamma_j$ is the strength of the jth vortex and K_{ij} is an aerodynamic kernel function that is given in [5].

As described by Deman Tang et al. [4], there are three sets of equations in the wake. At the first vortex in the wake, at time step $t+1$, one has:

$$\Gamma_{km+1}^{t+1} = -\sum_j^{km}(\Gamma_j^{t+1} - \Gamma_j^t). \tag{2}$$

Once the vorticity has been shed into the wake, it convects in the wake with speed U. From the second vortex point to the last two vortex points in the wake, for the special case where $\Delta x = U\Delta t$, this convection is described numerically by:

$$\Gamma_i^{t+1} = \Gamma_{i-1}^t, \quad i = km+2, ..., kn-1. \tag{3}$$

At the last vortex point in the wake, one has the following relationship for the vortex distribution:

$$\Gamma_i^{t+1} = \Gamma_{i-1}^t + \alpha\Gamma_i^t \quad i = kn, \tag{4}$$

where α is a relaxation factor; usually $0.95 < \alpha < 1.0$.

Putting together Equations 1 to 4 gives an aerodynamic matrix equation:

$$A\Gamma^{t+1} + B\Gamma^t = w^{t+1}, \tag{5}$$

where A and B are aerodynamic coefficient matrices. From fundamental aerodynamic theory, one can obtain the pressure distribution on the plate at the jth point, in terms of the vortex strength, as:

$$\Delta p_j = \frac{\rho_\infty}{\Delta x}\left[U(\Gamma_j^{t+1} + \Gamma_j^t)/2 + \sum_i^j \Delta x(\Gamma_i^{t+1} - \Gamma_i^t)/\Delta t\right]. \tag{6}$$

Let:

$$\overline{\Gamma} = \Gamma/(Uc), \quad U \equiv \Delta x/\Delta t,$$

and the overbar of Γ is then dropped for convenience. Thus, the nondimensional pressure is given by:

$$\Delta\overline{p}_j = \frac{c}{\Delta x}\left[\left(\Gamma_j^t + \Gamma_j^{t+1}\right)/2 + \sum_i^j \left(\Gamma_i^{t+1} - \Gamma_i^t\right)\right], \quad (7)$$

and the aerodynamic generalized force is calculated from:

$$Q^{ij} = \frac{\rho_\infty U^2 c^4}{Dh}\int_0^1\int_0^1 \Delta\overline{p}\phi_i\psi_j dxdy. \quad (8)$$

REDUCED-ORDER AERODYNAMIC MODEL (EIGENMODES)

If one assumes the structural response to be zero, then, from Equation 5 one can obtain a representation of unforced fluid motion as:

$$A\Gamma^{t+1} + B\Gamma^t = 0. \quad (9)$$

From Equation 9, an aerodynamic eigenvalue problem may be found. Because the matrices A and B are nonsymmetric, the right and left eigenvalues and eigenvectors of the generalized eigenvalue problem must be computed. They are :

$$AXZ = -BX, \quad (10)$$

and:

$$A^T YZ = -B^T Y, \quad (11)$$

where X and Y are the right and left eigenvector matrices and Z is a diagonal matrix whose diagonal entries contain the eigenvalues. The discrete-time eigenvalues, z_i, are related to continuous-time eigenvalues, λ_i, by $z_i = \exp(\lambda_i \Delta t)$. The real part of λ_i indicates the damping of the system and the imaginary λ_i provides the oscillation frequency. The right and left eigenvectors are orthogonal with respect to the matrices A and B. The eigenvectors are normalized such that they are orthonormal with respect to A. Therefore:

$$Y^T AX = I, \quad (12)$$

and:

$$Y^T BX = -Z. \quad (13)$$

Next, let the point vortex vector, Γ, be a linear combination of the Ra, right eigenvectors (where, in practice, $Ra << kn \times kmm$), i.e.:

$$\Gamma = X_{Ra}\gamma, \quad (14)$$

where γ is the vector of the aerodynamic modal coordinates.

One finds that with the reduced order aerodynamic model, only a few aerodynamic eigenmodes need to be retained in the aeroelastic model for good accuracy. However, whereas the dominant eigenmodes have been retained, all of the eigenmodes participate in the response to some degree. To account for the neglected eigenmodes, therefore, a quasistatic correction is used, which accounts for much of their influence. This technique is similar to the mode-acceleration method common to structural dynamics and was first suggested in the context of fluid eigenmode analysis by Florea and Hall [6]. Thus, let:

$$\Gamma = \Gamma_s + \Gamma_d = \Gamma_s + X_{Ra}\gamma_d, \quad (15)$$

where the first term on the right-hand side is a quasistatic solution of the vortex flow and the second term is a dynamic perturbation solution. By definition, the quasistatic portion, Γ_s, is given by:

$$[A + B]\,\Gamma_s^t = w^t, \quad (16)$$

where w^t is the downwash at time step t. Equations 5 and 16 may be inverted once to determine Γ_s^t, in terms of w^t and do not need to be evaluated at each time step.

NONLINEAR STRUCTURAL EQUATIONS

The nonlinear structural equations for a plate were derived from Hamilton's principle and Lagrange's equations. These equations are based on the Von Karman plate theory using total kinetic and elastic energies and the work done by applied aerodynamic loads on the plate [7]. Approximate modes are substituted into the energy expression and then into Lagrange's equations to yield equations of motion for each structural modal coordinate. The results are presented as follows.

STRUCTURAL MODE FUNCTIONS

The transverse or out-of-plane displacement, w, and the in-plane displacements, u and v, are expanded as follows:

$$u = \sum_i \sum_j a_{ij}(t)u_i(x)u_j(y),$$

$$v = \sum_r \sum_s b_{rs}(t)v_r(x)v_s(y),$$

$$w = \sum_m \sum_n q_{mn}(t)\phi_m(x)\psi_n(y), \quad (17)$$

where the mode functions $u_i, u_j, v_r, v_s, \phi_m$ and ψ_n are given by:

$$u_i(x) = \cos i\pi(x/c)$$

$$u_j(y) = \sin[(2j-1)/2]\pi(y/L),$$

$$v_r(x) = \cos r\pi(x/c),$$

$$v_s(y) = \sin[(2s-1)/2]\pi(y/L),$$

$$\phi_m(x) = \sqrt{2}\sin\left[\beta_m(x/c) + \frac{3}{4}\pi\right] + \exp\left[-\beta_m(x/c)\right] + (-1)^{m+1}\exp\left\{-\beta_m\left[1-(x/c)\right]\right\},$$

$$\psi_n(y) = \sqrt{2}\sin\left[\beta_n(y/L) - \frac{1}{4}\pi\right] + \exp\left[-\beta_n(y/L)\right] + (-1)^{n+1}\exp\left\{-\beta_n\left[1-(y/L)\right]\right\} + (-1)^n\exp(-\beta_n),$$

with:

$$\beta_m = (m-\frac{3}{2})\pi, \quad \beta_n = (n-\frac{1}{2})\pi,$$

$\phi_m(x)$ is a free-free beam function and $\psi_n(y)$ is a cantilever beam function. For $m < 2$, the rigid-body translation and the rotation modes are:

$$\phi_1(x) = 2, \quad \phi_2(x) = 2[1-2(x/c)],$$

and $a_{ij}, b_{rs}, q_{mn}, u, v$ and w are normalized by plate thickness, h and x and y by c and L, respectively.

IN-PLANE EQUATIONS

It is assumed that all of the nonconservative forces act in the z direction only and the in-plane inertia may be neglected. Thus, the in-plane equations of motion are determined from stretching strain energy and Lagrange's equation. The nondimensional in-plane u and v equations are, thus:

$$\sum_k\sum_p C^{ij}_{kp}a_{kp} + \sum_g\sum_f C^{ij}_{gf}b_{gf} = C^{ij},$$

$$\sum_k\sum_p D^{rs}_{kp}a_{kp} + \sum_g\sum_f D^{rs}_{gf}b_{gf} = D^{rs}, \tag{18}$$

where C^{ij} and D^{rs} are nonlinear (quadratic) functions of the plate transverse direction. The coefficient terms $C^{ij}_{kp}, C^{ij}_{gf}, D^{rs}_{kp}$ and D^{rs}_{gf} are, respectively:

$$C^{ij}_{kp} = 2\left(\frac{h}{c}\right)\int_0^1 u'_k u'_i dx \int_0^1 v'_p v'_j dy + (1-\nu)\left(\frac{h}{L}\right)^2\int_0^1 u_k u_i dx \int_0^1 v'_p v'_j dy,$$

$$C^{ij}_{gf} = 2\nu\frac{h^2}{cL}\int_0^1 u_g u'_i dx \int_0^1 v'_f v'_j dy + (1-\nu)\frac{h^2}{cL}\int_0^1 u'_g u_i dx \int_0^1 v_f v'_j dy,$$

$$D^{rs}_{kp} = 2\nu\frac{h^2}{cL}\int_0^1 u'_k u_r dx \int_0^1 v_p v'_s dy + (1-\nu)\frac{h^2}{cL}\int_0^1 u_k u'_r dx \int_0^1 v'_p v_s dy,$$

$$D^{rs}_{gf} = 2\left(\frac{h}{L}\right)^2\int_0^1 u_g u_r dx \int_0^1 v'_f v'_s dy + (1-\nu)\left(\frac{h}{c}\right)^2\int_0^1 u'_g u'_r dx \int_0^1 v_f v_s dy,$$

and the terms C^{ij} and D^{rs} are given in [8].

TRANSVERSE EQUATIONS

The transverse equation is formed by substituting the kinetic, bending and stretching energy expressions into Lagrange's equation. The nondimensional equation is:

$$\sum_m\sum_n\left[A^{ij}_{mn}\ddot{q}_{mn}(\tau) + B^{ij}_{mn}q_{mn}(\tau)\right] + F^{ij} + Q^{ij} = 0. \tag{19}$$

That is:

$$[A]\{\ddot{q}\} + [B]\{q\} + \{F\} + \{Q\} = 0, \tag{20}$$

where:

$$A^{ij}_{mn} = \frac{1}{6}\int_0^1\phi_m\phi_i dx\int_0^1\psi_n\psi_j dy,$$

$$B^{ij}_{mn} = \frac{1}{6}\left\{\int_0^1\phi''_m\phi''_i dx\int_0^1\psi_n\psi_j dy + \left(\frac{c}{L}\right)^4\int_0^1\phi_m\phi_i dx\int_0^1\psi''_n\psi''_j dy + \nu\left(\frac{c}{L}\right)^2\left[\int_0^1\phi_m\phi''_i dx\int_0^1\psi''_n\psi_j dy + \int_0^1\phi''_m\phi_i dx\int_0^1\psi_n\psi''_j dy\right] + 2(1-\nu)\left(\frac{c}{L}\right)^2\int_0^1\phi'_m\phi'_i dx\int_0^1\psi'_n\psi'_j dy\right\},$$

F^{ij} is a nonlinear force that depends on the deflection of the plate. Q^{ij} is the nondimensionalized, generalized aerodynamic force, which was discussed earlier.

AEROELASTIC MODEL

Having discussed the reduced order modeling technique earlier, a brief description is now given of how to incorporate the reduced order aerodynamic model, with the structural model discussed in the last part, into an aeroelastic model of flutter. Consider a discrete-time history of plate motion, $q(t)$, with a constant sampling time step, Δt. The sampled version of $q(t)$ is then described by:

$$q = \frac{(q^{t+1} + q^t)}{2}, \tag{21}$$

and the velocity of this discrete-time series is defined by:

$$\dot{q} = \frac{(q^{t+1} - q^t)}{\Delta t}. \tag{22}$$

The structural dynamic, Equation 19, can be reconstituted as a state-space equation in discrete-time form. It is given by:

$$D_2\boldsymbol{\theta}^{t+1} + D_1\boldsymbol{\theta}^t + C_2\boldsymbol{\Gamma}^{t+1} + C_1\boldsymbol{\Gamma}^t = -F_N^{t+\frac{1}{2}}, \tag{23}$$

where the vector, $\boldsymbol{\theta}$, is the state of the plate, $\{\boldsymbol{\theta}\} = \{\dot{q}, q\}$ and D_1 and D_2 are matrices describing the plate structural behavior. $C_1$and C_2 are matrices describing the vortex element behavior on the plate itself. There is a linear relationship between the downwash, w, at the collocation points and plate response, $\boldsymbol{\theta}$. It is defined by:

$$\mathbf{w} = \mathbf{E}\boldsymbol{\theta}. \tag{24}$$

Thus, combining Equations 5, 23 and 24, one obtains the aeroelastic state-space model in matrix form:

$$\begin{bmatrix} A & -E \\ C_2 & D_2 \end{bmatrix} \begin{Bmatrix} \boldsymbol{\Gamma} \\ \boldsymbol{\theta} \end{Bmatrix}^{t+1} + \begin{bmatrix} B & 0 \\ C_1 & D_1 \end{bmatrix} \begin{Bmatrix} \boldsymbol{\Gamma} \\ \boldsymbol{\theta} \end{Bmatrix}^{t} = \begin{Bmatrix} 0 \\ -F_N \end{Bmatrix}^{t+\frac{1}{2}}. \tag{25}$$

Equation 25 is referred to as the complete fluid/structure model. The eigenvalues of the homogeneous part of Equation 25 determine the stability of the aeroelastic system. If any of the eigenvalues have magnitude greater than unity, then the system is unstable. In principle, one could find the eigenvalues of Equation 25 directly. However, for most aeroelastic calculations, one must compute the eigenvalues of the system as a function of some parameters such as the reduced velocity. Under these circumstances, it is computationally much more efficient to model the unsteady aerodynamic loads using the reduced order aerodynamic model presented in earlier parts. Changing to normal mode coordinates (see Equation 14) and premultiplying the upper portion of Equation 25 by Y_{Ra}^T, gives:

$$\begin{bmatrix} I & -Y_{Ra}^T E \\ C_2 X_{Ra} & D_2 \end{bmatrix} \begin{Bmatrix} \gamma \\ \theta \end{Bmatrix}^{t+1} + \begin{bmatrix} -Z_{Ra} & 0 \\ C_1 X_{Ra} & D_1 \end{bmatrix} \begin{Bmatrix} \gamma \\ \theta \end{Bmatrix}^{t} = \begin{Bmatrix} 0 \\ -F_N \end{Bmatrix}^{t+\frac{1}{2}}. \tag{26}$$

Finally, incorporating the static correction technique into the reduced order aerodynamic model and after some manipulation, one obtains:

$$\begin{bmatrix} I & -Y_{Ra}^T[I - A(A+B)^{-1}E] \\ C_2 X_{Ra} & D_2 + C_2(A+B)^{-1}E \end{bmatrix} \begin{Bmatrix} \gamma_d \\ \theta \end{Bmatrix}^{t+1} + \begin{bmatrix} -Z_{Ra} & -Y_{Ra}^T\left[B(A+B)^{-1}\right]E \\ C_1 X_{Ra} & D_1 + C_1(A+B)^{-1}E \end{bmatrix} \begin{Bmatrix} \gamma_d \\ \theta \end{Bmatrix}^{t} = \begin{Bmatrix} 0 \\ -F_N \end{Bmatrix}^{t+\frac{1}{2}}. \tag{27}$$

The eigenvalues of Equation 27 will closely approximate the eigenvalues of Equation 5, provided that a sufficient number of eigenmodes are retained in the model.

NUMERICAL RESULTS

Equation 27 is a set of nonlinear ordinary differential equations. Note that the nonlinear F_N include, not only the generalized coordinates, q_{mn}, but also, a_{ij} and b_{rs}. Equations 18 and 19 are algebraic equations. If q_{mn} is given, the generalized coordinates a_{ij} and b_{rs} obtained from Equation 18 can be substituted into Equation 17. Then, Equation 19 can be solved by the Runge-Kutta method, step by step in time. Four rectangular cantilever plate models of varying aspect ratio were considered. The models are taken to be an aluminum alloy plate of constant thickness with aspect ratios of $AR \equiv L/c = 0.75 - 10$. The plate streamwise length, $c = 0.3$ m is fixed. The plate thickness is $h = 0.001$ m and Poisson's ratio is $\nu = 0.3$. For the basic case, the plate was modeled using 50 vortex elements, i.e., $km = 10$ and $kn = 5$. The wake was modeled using 150 vortex elements, i.e., $kmm = 40$. The total number of vortex elements (or aerodynamic degrees of freedom) is 200. The plate modal numbers are $nx = 4, ny = 2, mx = 10$ and $my = 2$. The vortex relaxation factor was taken to be $\alpha = 0.992$.

VORTEX LATTICE MODEL

The results in this section are presented to validate the unsteady vortex lattice model. Figure 2 shows the

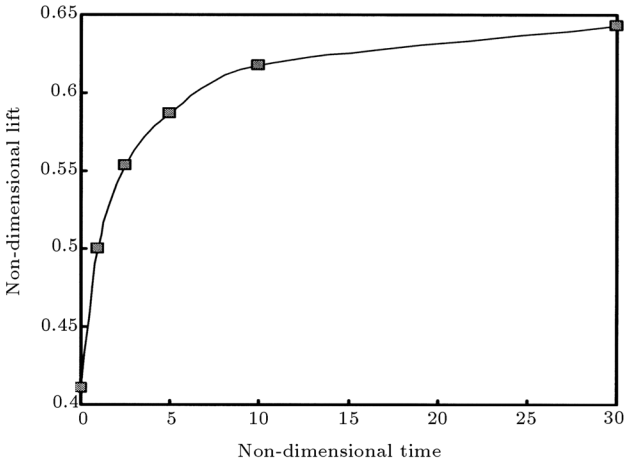

Figure 2. Time history lift due to step change in downwash for plate.

indicial response of a rectangular wing with an aspect ratio of 5.0, due to the rigid-body plunging motion of the wing.

To reduce the number of vortex elements required, the solution was assumed to be symmetric about the longitudinal axis.

For this example, the wing was modeled with 8 vortex elements in the streamwise direction and 10 in the spanwise direction. The wake was taken to be five chords long and was modeled using 40 vortex elements in the streamwise direction and 10 in the spanwise direction. The wake relaxation factor, α, was set to 0.992.

EIGENMODES OF AERODYNAMIC SYSTEMS

Typical eigenvalues for the basic vortex lattice model are shown in Figure 3. This figure shows eigenvalues in terms of discrete time multiplier, Z. Note that for normalization purposes, the airspeed, U, is assumed to be unity and, thus, $\Delta t = \Delta x$.

There are 64 real and 136 complex conjugate eigenvalues. When the wake elements are increased (note that the number of spanwise vortex locations kn does not change), the eigenvalues become denser in their distribution. A numerical example is shown in Figure 4 for $km = 40$ and $kmm = 160$. To determine the contribution of the individual aerodynamic eigenmodes to overall wing lift, a numerical experiment was considered. It is assumed that the wing plate is absolutely rigid and a unit step change in downwash is prescribed over the wing. The lift is defined as:

$$C_L = \frac{1}{\rho_\infty U^2} \int_0^1 \int_0^1 \Delta p(x,y) dx dy, \tag{28}$$

the results for C_L are shown in Figure 5 [9].

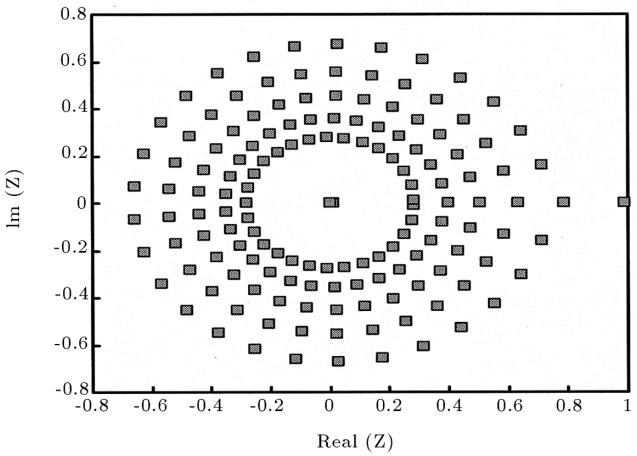

Figure 3. Eigenvalue solutions of vortex lattice model of unsteady flow about a three-dimensional plate: $kn = 5, km = 10$ and $kmm = 40$.

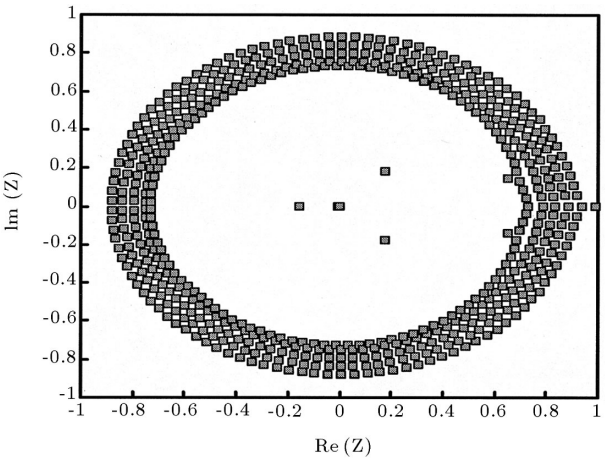

Figure 4. Eigenvalue solutions of vortex lattice model of unsteady flow about a three-dimensional plate: $kn = 5, km = 40$ and $kmm = 160$.

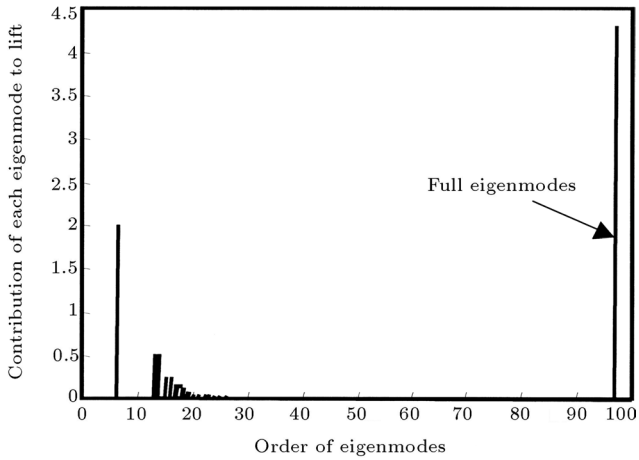

Figure 5. Contribution of each aerodynamic eigenmode to overall wing lift [9].

Figure 5 shows the magnitude of the lift created by individual aerodynamic eigenmode $C_L(i)$ vs the aerodynamic eigenmode number i.

For comparison, the total lift created by all eigenmodes, $C_{L,\text{total}}$, is also plotted in Figure 5, as shown by the thick bar. Only 90 aerodynamic eigenmodes are plotted in Figure 5 because, beyond 90 eigenmodes, the lift contribution is almost zero. The first 12 eigenmodes plotted are from the pure real eigenvalues and the order is from smaller to larger damping. It is seen that the first important contribution is from the 6th eigenmode and the second most important is from the 13th eigenmode. The contribution decreases as the eigenmode order, i.e., damping, increases. For the pure real eigenmodes, the eigenmodes with the smallest damping are not always the most important. For the present example, only a few eigenmodes are significant, which provides very useful information for the flutter analysis using the reduced-order aerodynamic model.

REDUCED ORDER AERODYNAMIC MODELS

The eigenmode information computed in the previous section is now used to construct reduced order aerodynamic models. One considers the case of the finite wing vibrating with a rigid-body plunging motion. Two reduced order models were used; both contained 39 eigenmodes, but one used the static correction technique and one did not. Figure 6 shows the unsteady lift as a function of reduced frequency. The results show that the reduced order model using static correction agrees well with the direct vortex lattice solver, whereas the reduced order model without static correction has significant errors at high reduced frequencies. One interesting feature of the case shown in Figure 6 is that most of the eigenmodes used in the reduced order model were eigenmodes of the first mode branch cut

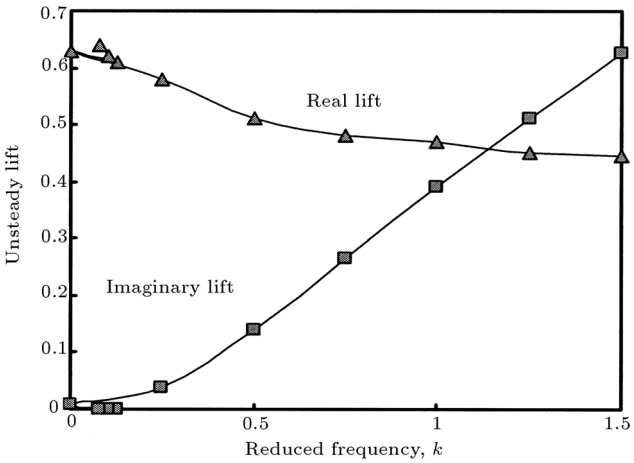

Figure 6. Unsteady lift due to harmonic rigid body plunging motion of plate.

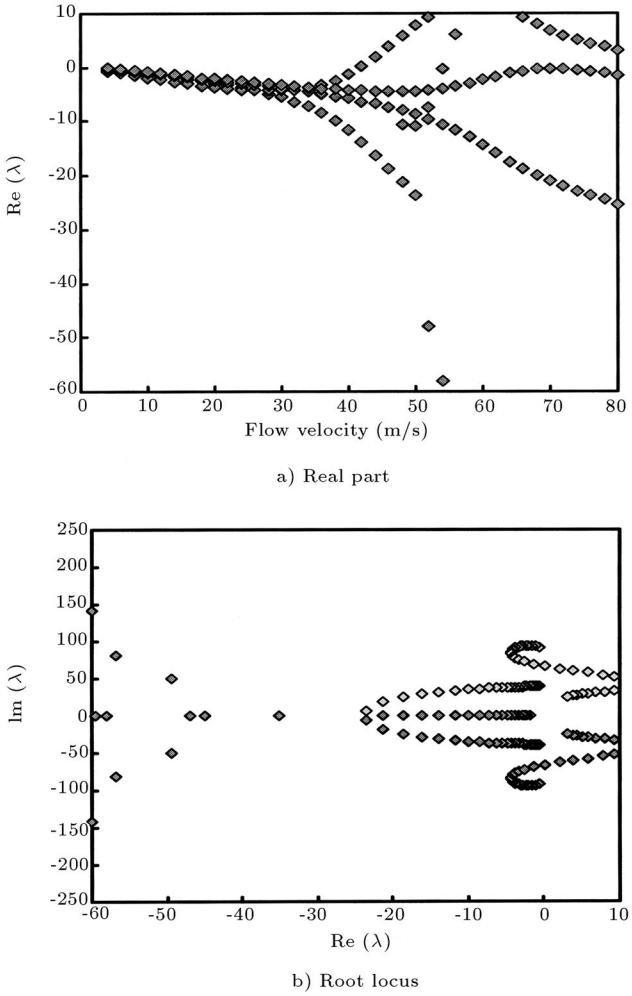

Figure 7. Eigenvalue solutions of linear aeroelastic model.

(the branch cut nearest the imaginary axis). This suggests that one might be able to reduce the size of the vortex lattice model by using vorticity distributed in a few appropriately shaped spanwise modes.

Another interesting point is that no more modes were required to obtain satisfactory results for a finite wing than were required for two-dimensional, even though the wing has a total of 480 degrees of freedom.

FLUTTER CALCULATIONS

Next, one considers the use of reduced order models to compute the flutter stability of a cantilever plate. When the nonlinear force, F_N, in Equations 25, 26 or 27, is set to zero, a linear aeroelastic model is obtained. The aeroelastic eigenvalues from solving these equations determine the stability of the system. When the real part of any eigenvalue, λ, becomes positive, the entire system becomes unstable. Figures 7a and 7b show a typical graphical representation of the eigenanalysis in the form of real eigenvalues, $Re(\lambda_i)$, vs the flow velocity and, also, a root-locus plot for the nominal

linear system using all aerodynamic eigenmodes. There are two intersections of $Re(\lambda_i)$ with the velocity axis. One is $U_f = 42$ m/s, for the critical flutter velocity with the corresponding flutter oscillatory frequency $\omega_f = 76.8$ rad/sec. The other is $U_d = 54.3$ m/s, for the divergent velocity with zero oscillatory frequency. Note that the divergent velocity corresponds to a primarily aerodynamic mode. Figure 8 shows a graphical representation of the eigenanalysis using a reduced-order aerodynamic model with a static correction for seven aerodynamic eigenmodes ($Ra = 7$), i.e., the 6th and 13th-18th eigenmodes corresponding to Figure 5. Excellent agreement between the full and the reduced aerodynamic eigenmode results is obtained. However, the computation time using the reduced-order model is only about $\frac{1}{150}$ that of the original model.

From Figure 7, it is found that the linear flutter motion is dominated by the coupling between the first two structural modes, i.e., the spanwise bending mode and the rigid plunge and rotation modes in the chordwise direction. Figure 8 shows the flutter velocities (Figure 8a) and frequencies (Figure 8b) of the linear system vs the aspect ratio $AR \equiv L/c$ from 0.75 to 10, using a five-eigenmode, reduced-order aerodynamic model (6th and 13th-16th) with a static correction. Both flutter velocity and corresponding frequency are increased as the aspect ratio decreases. It was found that the results for the five and seven reduced-order aerodynamic modes are virtually identical.

Figure 9 shows the convergent behavior of the linear flutter velocity vs the numbers of the structural modal function, nx and ny. Figure 9a is for the flutter velocities and Figure 9b is for the correspondent frequencies of the linear system. The present method has good convergence, both for $ny = 1$ and $ny = 2$, when $nx > 3$. Note that the flutter velocities for $ny = 1$ are modestly higher than those for $ny = 2$. It is found that for $AR \equiv 1$, when $ny = 1$ and $nx = 3$, the first three plate natural frequencies are 6.5, 18.2 and 58.9 Hz. Thus, it is found that there is a lower second natural frequency of the plate for $ny = 2$, as compared with $ny = 1$. This leads to a lower flutter velocity for

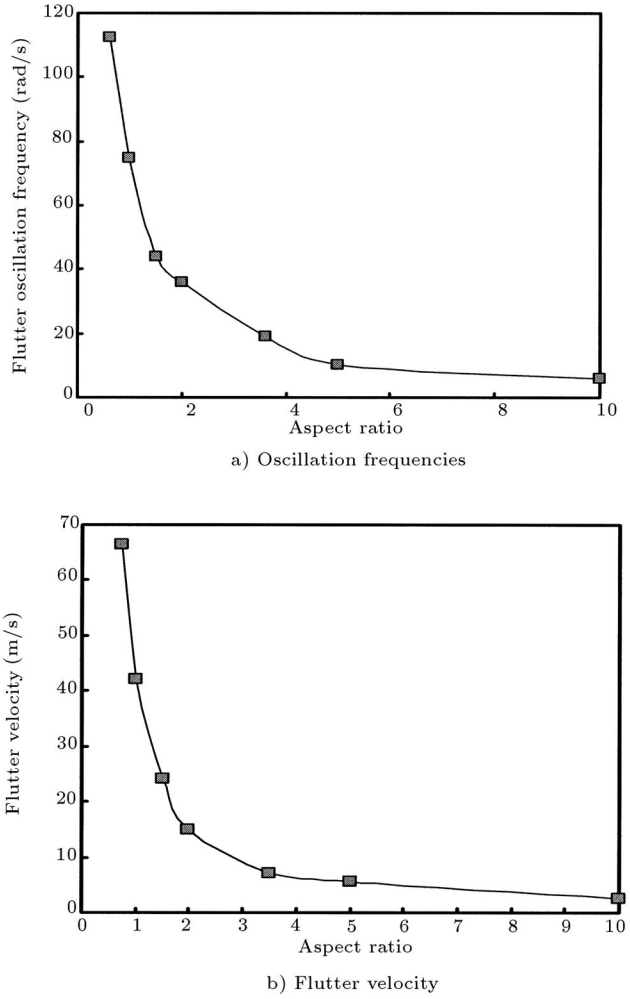

Figure 8. Linear aeroelastic model vs aspect ratio of the plate.

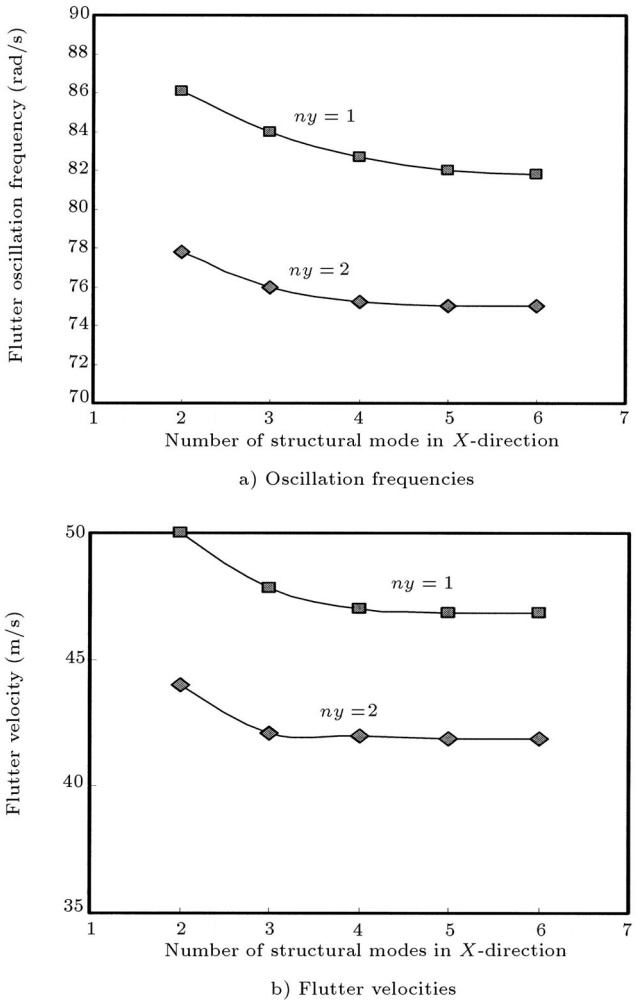

Figure 9. Linear aeroelastic model vs the numbers of structural modal function.

$ny = 2$. The results for $ny = 3$ are essentially the same as for $ny = 2$.

CONCLUSIONS

Vortex lattice aerodynamic theory has been used to construct a reduced-order aerodynamic model about a three-dimensional cantilever plate. It was shown that the unsteady fluid motion could be modeled accurately using just a small number of aerodynamic eigenmodes. A static correction is applied to approximate the influence of the remaining eigenmodes. Such a reduced order model is particularly useful when a large number of calculations are to be performed. The present method has good accuracy and computational efficiency for both linear flutter and nonlinear response analysis.

The present paper provides new insight into a nonlinear aeroelastic phenomenon not previously widely appreciated for low aspect ratio wings that have a plate-like structural behavior. Comparing the results obtained in the present paper with those of [1], verifies the accuracy of the present method for a 3-D aerodynamic model.

REFERENCES

1. Davis, G.A. and Bendiksen, O.O. "Unsteady transonic two-dimensional Euler solutions using finite elements", *AIAA Journal*, **31**(6), pp 1051-1059 (1993).
2. Batina, J.T. "Unsteady Euler algorithm with unstructured dynamic mesh for complex-aircraft aerodynamic analysis", *AIAA Journal*, **29**(3), pp 327-333 (1991).
3. Chaderjian, N.M. and Guruswamy, G.P. "Transonic Navier-stokes computations for an oscillating wing using zonal grids", *Journal of Aircraft*, **29**(3), pp 326-335 (1992).
4. Tang, D., Dowell, E.H. and Hall, K.C. "Limit cycle oscillations of a cantilevered wing in low subsonic flow", *AIAA Journal*, **37**(3), pp 364-371 (March 1999).
5. Bertin, J.J. and Smith, M.L., *Aerodynamic for Engineers*, Second edition, Prentice-Hall, International Editions, pp 271 (1989).
6. Florea, R. and Hall, K.C. "Reduced order modeling of unsteady flows about airfoils", *Aeroelasticity and Fluid Structure Interaction Problems*, P.P Friedmann and J.C.I. Chang, Eds., **44**, American Society of Mechanical Engineers, New York, USA, pp 49-68 (1994).
7. Dowell, E.H., *Aeroelasticity of Plates and Shells*, Kluwer, Dordecht, The Netherlands, pp 35-49 (1975).
8. Weiliang, Y. and Dowell, E.H. "Limit cycle oscillation of a fluttering cantilever plate", *AIAA Journal*, **32**(12), pp 2426-2432 (1994).
9. Hall, K.C. "Eigenanalysis of unsteady flow about airfoils, cascades, and wings", *AIAA Journal*, **32**(12), pp 2426-2432 (1994).